INFLUENCE OF CERIA DOPING ON STRUCTURAL AND OPTICAL PROPERTIES OF TIN OXIDE NANOPARTICLES

Sachin T. Bahade[1], Amrut S. Lanje[2], Satish J. Sharma[3], Amresh I. Prasad[4]
[1,2]Department of Electronics, Dr. Ambedkar College, Chandrapur (M.S.), India
[3]Department of Electronics, R. T. M Nagpur University, Nagpur (M.S.), India
[4]Department of Nanotechnology, North Eastern Hill University, Shilong, Meghalaya, India

ABSTRACT:
In this paper, the synthesis of Ceria doped SnO_2 nanopawder (Ce:SnO_2) has been introduced by sol gel method using non-alkoxide $SnCl_4.2H_2O$, CeO_2 as a precursors. The structural and optical properties of the prepared Ce:SnO_2 powder sample has been carried out as a function of annealing temperature. The X-ray Diffraction (XRD), shows the samples have a tetragonal rutile structure with some Ce impurity peaks. The Transmission Electron Microscopy (TEM) shows the average particle size is of ~19 nm for wt. at 5%. The Chemical Bonding, Functional group and optical characteristics were investigated using FT-IR, Uv-vis and PL.
Keywords: Sol gel, Ce:SnO_2 Nanoparticles, Optical

1.INTRODUCTION

In recent years, Tin oxides a sort of n-type semiconductor material have attracted a lot of interest due to their fascinating features, i.e high surface-to-volume ratio[1], strong carrier confinement[2], enhanced surface modes in their Raman spectra and high transmittance and electrical conductivity. These properties leads to applications in catalysis, gas sensing, and optoelectronics such as light emitting diode, Solar cells and panel displays [3,4] etc. Though a considerable effort has been given to obtain stoichiometric pure and Ce doped SnO_2 nanoparticles at different concentration. The structural and optoelectronic properties have been investigated. The applied synthesis procedures have seen to affect substantially the crystallinity, microstructure and defect structure of the nanocrystals. Several methods including sol-gel [5], hydrothermal [6], electrospinning [7] have been utilized to synthesize SnO_2. Among these techniques, the sol gel method seems suitable due to its simplicity, easy to add doping materials, promising for mass production and low cost. The properties of doped SnO_2 were found to be dependent on the processing conditions and nature of precursors used. The precursors play an important role in Growth, the structure the morphology as well as optical and electrical characteristics of the doped material. Recently, the rare earth doped semiconductor materials like La, Er, Ce, Yb have attracted much attention because of their applications in Optoelectronic devices [8]. Due to the limitation of solubility, these ions acts as grain growth inhibitors and remain aggregates at the grain boundaries. Although, to date there is few work has been carried out to investigate optical properties using Ce doped SnO_2. In the present work, sol gel synthesis method employed to obtain pure and Ce doped Nanocrystals at 500^0C. The effect of pure and with Ce doped tin oxide is on Structural, Morphological and Optical characteristics were studied.

2. MATERIALS AND METHODS:

Nanocrystalline Ce doped SnO_2 samples were prepared by a Sol gel rout using Sn and Ce precursors taken in the form of chlorides and oxide respectively. In a typical synthesis process of Pure and doped SnO_2, dissolve 8g of

$SnCl_4$. $2H_2O$ from Merck, India in 100 ml ethanol solution (Ethanol+Water 1:1) and Stirred about 20 min until a transparent sol is produced. In order to investigate the effect of Ce dopant on structural and Optical properties, Ceric Oxide, A.R Himedia Laboratories Pvt. Ltd. from Burgoyne Burbidge's & Co. Mumbai (India) was Added to the solution and stirred for 30 min. at different concentration at wt. 0%, 1%, 3%, 5%, 7%. Add aqueous Ammonia solution (25% merck, India) dropwise to the solution under constant stirring and PH of solution was adjusted to a value upto 8. After 24 Hr of aging in the air resulting opal gel were Centrifused and washed with Ethanol at least 5 times to remove ammonia, chloride impurity. The collected gel was dried in furnace over 80^0C/4Hr in the air to remove moisture. Then after crush the sample and Sintered at 500^0C/4 Hr. Finally ashed coloured nanoparticle powders were formed [5].

The structure of Ce:SnO_2 synthesized nanoparticles were Characterized by X-ray diffractometer (Bruker D8 Advance). The surface morphology & grain sizes observed by Scanning Electron microscopy(JEOL JSM 5600) and Transmission electron microscopy (JEOL/JEM 2100). FT-IR spectra of the powders were recorded using a Bruker, Germany, Model vertex 70 using the KBr pellet technique in the range 400 to 4000 cm^{-1}. Photoluminescence (PL) studies of prepared samples were carried out using a F-4500 FL spectrometer. UV-Vis measurement was recorded using Jasco Spectrophotometer V-770 in a 200-1000 wavelength domain.

3. RESULT AND DISCUSSION

3.1 Structural investigation

XRD

To study the crystallite size, crystal structure and lattice parameters of Ce doped SnO_2, XRD analysis was used. The X-ray diffraction patterns of pure and Ce doped SnO_2 nanoparticles with various concentration sintered at 500^0C shown in Fig.1. The peaks were indexed using Powder X software and they are matched with the tetragonal rutile structure of SnO_2, which are consistent with the values in the standard card (JCPDS 77-0452) with a maximum intensity corresponding to (110) plane [9].

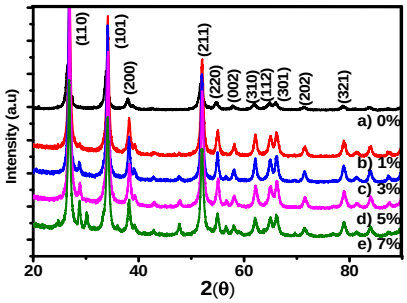

Figure 1 : **a) XRD graph of Ce:SnO_2 at 0%, 1%, 3%, 5%, 7%.**

Table 1: XRD Data of Ce doped SnO_2 samples and Pristine SnO_2 sample.

Sample name	Crystal size(nm)	a (A^0)	c (A^0)	c/a	Volume
0%	33	4.711	3.171	0.6730	70.404
1%	22	4.715	3.170	0.6724	70.519
3%	26	4.713	3.175	0.6739	70.541
5%	25	4.710	3.169	0.6728	70.336
7%	23	4.715	3.170	0.6724	70.519

Very few impurity peak were observed in doped samples at 3%, 5%, 7% sintered at 500^0C, and indicating cubic structure of CeO_2(JCPDS 43-1002). The result shows that the intensity of peaks has been narrowed significantly, as the Ce concentration increases (1%, 3%, 5%, 7%) and all peaks showing clearly. Further it has been observed that lattice parameters a and c are calculated using unit cell software program and cell volume as shown in (Table 1). All calculated values are in good agreement with the reported values (JCPDS 77-0452). It can be seen that an increase or decrease of the lattice parameters "a" and unit cell volume, related to doping concentration in SnO_2. It may be attributed to the difference between ionic radius of Sn and Ce, which leads to stress in the host lattice and affect the crystalline nature of the material. The secondary phase can not be observed may be due to Ce content dispersed uniformly in SnO_2. There are two possible mechanisms involved in the narrowing/broadening of the peaks, one is the particle size effect and other is lattice strain. In available literature we found that, some authors reported successful insertion Ce ion in the oxide lattice, while others are reported that Ce ions can not be incorporated into crystals [10]. So, it

strongly depends on preparation technique and doping concentration.

The average size of the crystalline grains of the sample was calculated using at full width half-maximum (FWHM) and Debye-Scherer's formula [11] given by :

$$D_{hkl} = \frac{0.9\lambda}{\beta\cos\theta}$$

Here, D_{hkl} is the crystalline size, □□is the X-ray wave length, □□is the (110) full width at half maximum (FWHM) and □□is the angle of diffraction. The estimated sizes at the most intense crystallographic plane (110) are given in Table 1. The crystallite size of the pure and Ce doped SnO_2 nanoparticles are lying between 22-26 nm. The internal stress, strain, lattice distortion or defects can also affect the XRD peaks along with particle size [12]. This shows the limited solid solubility of Ce in SnO_2. It contributes two effects. First, to decrease of surface energy and lower the driving force [13]. Second, Tin oxide nanoparticles segregate from each other before the particles have grown into bigger size. Therefore, the thermal stability of the doped system can be improved and its boundary motion will be suppressed [14]. The authors found that the oxides like TiO_2, ZnO, CuO can disperse on to the surface of Tin Oxide causing a decrease in crystallite size. The incorporation of Ce into Tin oxide by the formation of Sn-O-Ce bond on the surface of small particles. This increases the stabilization of the small particles and confirming the role of Ce as a grain growth inhibitor [15]. The ratio of the lattice parameters a and c is a measure of lattice distortion, it has been calculated from XRD data (Table 1). The a/c ratio appears as constant in all the samples which that the lattice distortion is independent of Ce concentration in our samples. This suggest that all the atomic layers are equally strained at any Ce concentration. From the above discussion, it can be concluded that the narrowing or broadening of the XRD peaks of SnO_2 nonoparticles occurred due to atomic diffusion and lattice strains and not by lattice distortions. The particle size calculated by Scherrer formula for Ce:SnO_2 at 5 % have been further validated by Transmission Electron Microscopy(TEM) observations. Increase in Unit cell volume shows expansive strain in the particles and decrease in unit cell volume shows compressive strain in the particles.

3.2 SEM/TEM

Fig.3 shows the typical morphology and composition of pure and Ce:SnO_2 nanoparticles at wt. 1%, 3%, 5%, 7%. Powder samples were used for SEM analysis. Powder was stick on the sample holder using double sided tape and gold coated with sputter coater.

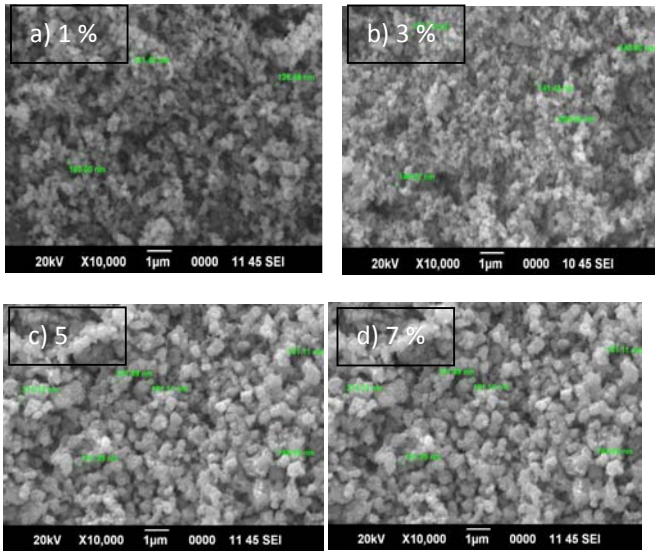

Figure 3 : SEM images of Ce:SnO_2 at 1%, 3%, 5 %, 7%.

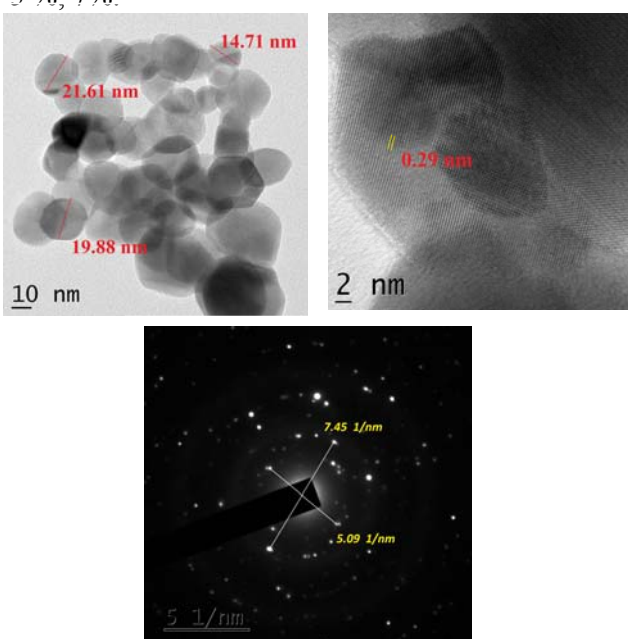

Figure 4 : TEM images of Ce:SnO_2 at 5 %.

It is seen that SEM image of Ce doped SnO_2 of all microstructure of these powder

samples shows the presence of small spherical aggregates of smaller individual nanoparticles with variations in particles size. Due to the large surface and high surface energy of primary nanoparticles, Tin Oxide tiny particles are prone to aggregated [16]. The enhancement of grain size with doping level confirms the presence of Ce ions into SnO_2 crystal which bothers the particle growth. The randomly grown grains gives rise in scattering effect, which reduces the transmittance [17]. The surface state of such oxide nanoparticles influence there optical and electrical properties which are essential to ensure the implementation of the different optoelectronic devices and gas sensors.

Fig.4 Shows TEM image of prepared Ce doped SnO_2 nanoparticles at 5% showing an average diameter of about ~19 nm as well. For this powder samples were dispersed in ethanol and sonicated in an ultrasonic bath. The particle size obtained from TEM analysis is slightly less than the crystalline size calculated from XRD data.

3.3 FT-IR STUDY

To investigate the functional groups and chemical bonding in the material Fourier transform infrared (FTIR) spectroscopy was carried out. The FT-IR spectra were recorded in solid phase at room temperature by using KBr pellets technique in the region of 400-4500cm^{-1}. FT-IR spectra of pure and Ce doped SnO_2 nanoparticles at 0%, 1%, 3%, 5%, 7% prepared at 500^0C are shown in Fig.5, and it is clear from the figure that there are clear changes in the shapes and positions of IR peaks indicating that Ce might have been incorporated in SnO_2 host. The observed frequency at 450 cm^{-1} is assigned to the symmetric Sn-O-Sn stretching mode. Antisymmetric Sn-O-Sn stretching mode of the surface hydroxyl groups is obtained at 650 cm^{-1} is observed. The broad band between 500 to 800cm^{-1} due to the vibrations of Sn-O-Sn mode of tin oxide [5,18-19]. It is clear from the figure that the transmittance increases initially then decreases with the increase in doping concentration.

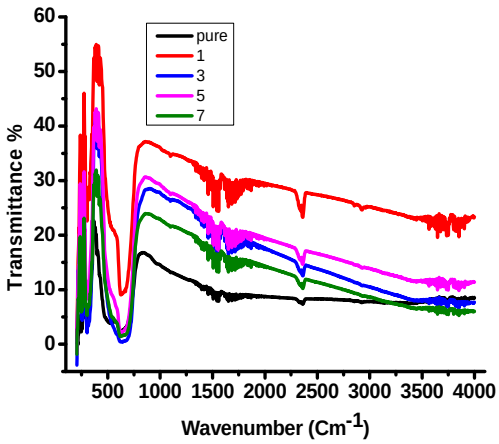

Figure 5 : FT-IR of pure and Ce:SnO_2

This might be due to the reducing the particle size with doping concentration. Secondly, the transmittance can also be attributed to the defects generated in the system.The peak at 800 cm^{-1} is related to the vibration of hydroxyl-tin (Sn-OH) bond. The vibrations from 1300-1700 cm^{-1} is assigned to the C-O stretching mode [20-21]. The bands appearing in all the samples around 1650 cm^{-1} might be due to the bending mode of O-H bonds. Lastly, the broad band appearing in the region 2500-3500 cm^{-1} may be due to vibration of adsorbed water. The present assignments corroborate well with the values very near to the reported available literature [22-24].

3.4 PHOTOLUMINESCENCE STUDY

The room temperature Photoluminescence behavior of pure and Ce doped SnO_2 nanoparticles was investigated using PL spectrometer. Fig. 5 contains the photo induced fluorescence spectra of all samples for an excitation wavelength 400 nm. It can be seen from the PL spectra the samples exhibit broad emission at 200 to 250 and one emission peak at 220 nm .

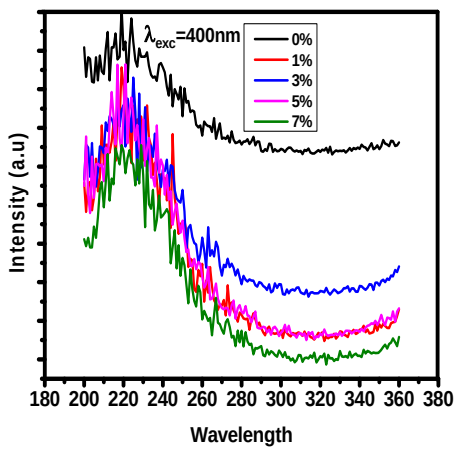

Fig. 5: PL emission spectra of pure and Ce:SnO_2

This emission bands presents due to essentially to the presence of point defects, such as oxygen vacancies in SnO_2 nanoparticles [25]. It can be seen from the Fig. 5 that there is slightly shift the PL peak position before or after the 220 nm as doping concentration increases. However, a slight increase in the intensity of luminescent emission was observed with doping which can be attributed to the defects such as oxygen interstitials and Ce vacancies in the doped samples.

3.5 UV-Vis STUDY

The optical absorption coefficient □(□) of Ce doped SnO_2 nanoparticles from 200 to 1000 nm range have been investigated. Fig. 6 shows plots of $(\alpha h\nu)^2$ versus photon energy (hν) for Ce:SnO2 nanoparticles and extrapolating the linear portion of these curves to find the intercept with photon energy axis. The band gap (Eg) is calculated from the Tauc's relation :

$$□h□ = A'(h□□ - Eg)^n$$

Where, □□is the absorption coefficient, A is a constant while the exponent n depends on the type of transition (n=2 for indirect allowed, n=1/2 for direct band gap semiconductor). Therefore, the optical band gap is obtained by extrapolation of the linear region of a tauc's plot.

The measured band gap E_g was found to be in the range of 3.04 to 3.32 eV, which is slightly small to the reported values of bulk SnO_2 i.e 3.6 eV It can be seen that the band gap values shows increase or decrease tendency with Ce doping content in Tin oxide structures. This can be attributed due to quantum confinement effect [26], reorientation effect [27], microstrain and dislocation density in nanoparticles.

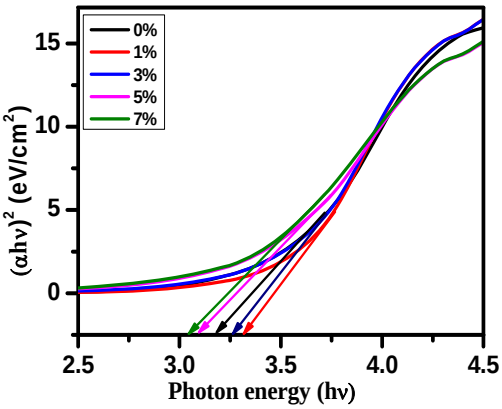

Fig. 6. Tauc's Plot of pure and Ce: SnO_2

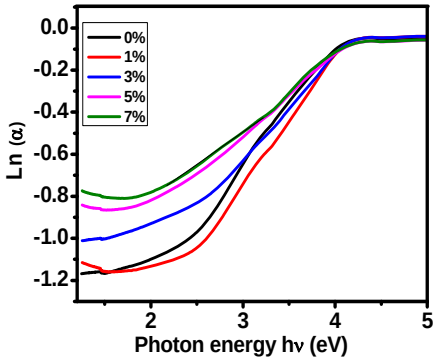

Fig. 7. Urbach Energy Plot of pure and Ce: SnO_2

The addition of impurity into semiconductors reveals band tailing in the band gap due to the formation of localized states. The charge carriers can hop from one to another site in the localized state.

Table 2: The calculated values of the Optical gap and Urbach energy

	0%	1%	3%	5%	7%
Eg(eV)	3.18	3.32	3.26	3.09	3.04
E_U(eV)	0.72	0.51	0.42	0.36	0.34

The Urbach E_U values were obtained from the inverse of the slop of Ln(□) Vs (h□) Fig. 7. and the calculated values are shown in Table 2. The Calculated values Urbach energy shows energy decreases as concentration

increases. This indicates that energy is associated with the micro-structural lattice disorder.

4. CONCLUSION AND OUTLOOK

This paper deals with some structural and optical characterization of obtained nanoparticles by sol gel method at 500^0C. First, the XRD study shows that the obtained powder have rutile tetragonal structure. Upon increasing the Ce doping concentration the crystalline quality was found to be affected. SEM images reveal the presence of agglomerates and a reduction in grain size with Ce content. TEM image 5 at % confirms its size closely matches with XRD value.

The IR Spectra shows that all the vibration broadens with the increase in doping concentration. PL emission shows slight increase in the intensity was observed with doping. Which contribute to the photocatalytic applications. UV-vis has successfully investigated to obtaine band gap and band tail value of doped material.

ACKNOWLEDGEMENT:

The author gratefully acknowledge the DST-SAIF, kochi for XRD, SEM, TEM measurement. We need to convey our thanks to Dr. R. S. Ningthoujam, Chemistry Division, BARC, Mumbai for PL & FT-IR measurement.

REFERENCES:

[1] N. S. Baik, G. Sakai, K. Shimane, N. Miura, and N. Yamazoe, (2000), Sens. & Actuators B, 65 (1-3), 97-100.

[2] E. J. H. Lee, C. Reibeiro, T. R. Giraldi, E. Longo and E. R. Leite, (2004), App. Phys. Lett., 84(10), 1745-1747.

[3] M. Epifani, J. Arbio, E. Pellicer, E. Comini, P. Siciliano, G. Faglia and J. R. Morante, (2008), Cryst. Growth Des. 8(5), 1774-1778.

[4] L .H. Qian, K. Wanga, H. T. Fang, Y. Lia, and X. L. Maa, (2007), Mater. Chem. Phys.,103(1), 132-136.

[5] A. S. Lanje, S. J. Sharma, R. B. Pode and R. S. Ningthoujam , Arch. Apll. Sci. Res., 2010, 2 (2):127-135.

[6] H. T. Chen, X. L. Wu, Y. Y. Zhang, J. Zhu, Y. C. Cheng and P. K. Chu,(2009), Appl. Phys. A, 97 (3), 581-585.

[7] Q. Qia, T. Zhanga, L. Liua and X. Zheng, (2009), Sens. Actuators B, 137(2), 471-475.

[8] R. Zamiri, A. F. Lemos, A. Reblo, H. A. Ahangar, J. M. F. Ferreira, Ceramics international 40 (2014) 523.

[9] A. D. Mighell, C. R. Hubbard, J. K Stalick, M. A. Holomany, NBS AIDS83 JCPDS-International Centre for Diffraction Data, Swarthmore, PA, U.S.A, 1983.

[10] J. Jia, F. Luo, C.Sau, X. Wang, H. Song, X. Hu, Ceramics International 40 (2014) 6973.

[11] B. D. Cullity, Elements of X-ray Diffraction (1978) A. W. Pub. Comp. Inc., Bostan.

[12] I. Navas, R. Vinodkumar, K. J. Lethy, M. Satyanarayana, V. Ganeshan and V. P. Mahadevan Pillai, J. Nanoscience and Nanotechnology. 9 (2009).

[13] A. P. Macial, P. N. Lisboa-Filho, E. R. Leite, C.O. Paiva-Santos, J. Eur. Ceram. Soc. 23 (2003) 707.

[14] G. T. Ang, G. H. Toh, M. Z. Abu Bakar, A.Z.Abdullah, M.R.Othman, Process Safety and Environmental Protection 89 (3) (2011) 186.

[15] M. M. Maletin, R. R. Denadi, L. M. Nikoli, V. V. Srdi, J. Optoelectron. Adv. Mater. 9 (7) (2007) 2245.

[16] L. Chao, W. Wei, X. Tanguchi, W. Huanxin, Z. Youqi, S. Yanliag, J. of Rare Earths 28 (2010) 161.

[17] F. Yakuphanouglu, Y.Caglar, S.Ilican, M.Caglar, Phys. B 394 (2007) 86.

[18] H. Frohlick, Theory of Dielectrics, Oxford University press (1956)

[19] P. I. Archer, P. V. Radovanovic, S. M. Heald and D. R. Gamelin, J. Am. chem. Soc. 127, 14479(2005)

[20] P. G. Horrison and A. J. Guest, J. Chem. Soc, Faraday Trans. 83 (1987) 3383.

[21] Z. Jun-Jei, Z. Jian-Min, L. Xue-Hong, F. Jiang-Lin, Miao-Gaozhou and C. Hong-Yuan, Mat. Lett. 53 (2002) 12.

[22] Jun-Jie Zhu, Jian-Min Zhu, X. Liao, J. Fang, M. Zhou, H. Chen, Mat. Lett. 53 (2003) 12.

[23] K. Srinivas, M. Vithal, B. Sreedhar, M. M. Raja and P. V. Reddy, J. Phys. Chem. C 113 (2009) 3543.

[24] P. G. Harrison and A. Guest, J. Chem. Soc, Faraday Trans. 183 (1987) 3383.

[25] S. Luo, J. Fan, W. Liu, M. Zhang Song, C. Lin, X. Wu and P. K. Chu (2006), Nanotechnology, 17(6) 1695-1699.
[26] T. Takagahara and K. Takeda, Phys. Rev. B, 46 (1992) 15578-15581.
[27] G. Turgut, E-F. Keskenler, Se. Aydin, E. Sonmez, S. Dogan, B. Duzgun, M. Ertugrul, Superlattices and Microstructures 56 (2013) 107.
[28] E. Burtein, Phy. Rev. 93 (1954) 632.
[29] J. F. Chang, H. H. Kuo, I. C. Leu & M. H. Hon, Sens. & Actuator B Chem.,84 (2002) 258-264.
[30] A. S. Lanje, S. J. Shrama, R. B. Pode, Arch. Phy. Res., 2010, 1 (1), 49.
[31] A. S. Lanje, S. J. Shrama, R. B. Pode, "Functional Nanomaterials Synthesis and Characterization" (2014) LAMBERT Aca. Pub., Germany.